

# Experimental and CFD Investigation on the Efficiency of Parabolic Solar Collector Involving Al<sub>2</sub>O<sub>3</sub>/H<sub>2</sub>O (DI) Nanofluid as a Working Fluid

Ketan Ajay\*<sup>‡</sup>, Lal Kundan\*\*,

\*Department of Mechanical Engineering, Thapar University, India

\*\*Department of Mechanical Engineering, Thapar University, India

(ketan.bhardwaj88@gmail.com)

<sup>‡</sup>Corresponding Author; Ketan Ajay, Department of Mechanical Engineering, Thapar University, India

ketan.bhardwaj88@gmail.com

Received: 20.01.2016 Accepted: 16.05.2016

**Abstract-**Nanotechnology plays a major role in heat transfer related problems. This study evaluates the effect of nanofluid as a working fluid on parabolic solar collector's overall efficiency through both experimental and CFD analysis.  $\alpha$ -Al<sub>2</sub>O<sub>3</sub> nanoparticle of 20 nm average size is used for the preparation of Al<sub>2</sub>O<sub>3</sub>-H<sub>2</sub>O (DI) nanofluid of four different volumetric concentrations of 0.05%, 0.75%, 0.1% and 0.125% respectively. Working fluid is made to flow at three different volume flow rates (30 LPH, 50 LPH and 80 LPH). ANSYS FLUENT 14.5 is used for carrying out CFD simulation, where solar flux is modelled through solar load cell and solar ray tracing. It has been observed that, there is improvement in instantaneous efficiency, thermal efficiency and in overall efficiency, when water is replaced by Al<sub>2</sub>O<sub>3</sub>-H<sub>2</sub>O (DI) nanofluid and also with corresponding increase in the mass flow rate of working fluid. An improvement of about 9.31%, 11.87%, and 13.98% in the collector's overall efficiency is seen, when water is replaced by 0.125% vol. conc. Al<sub>2</sub>O<sub>3</sub>-H<sub>2</sub>O (DI) nanofluid at a flow rates of 30 LPH, 50 LPH and 80 LPH respectively. Also, both experimental and CFD analysis results are in close agreement with a difference of 8%.

**Keywords** Solar energy, parabolic solar collector, nanofluid, CFD, Al<sub>2</sub>O<sub>3</sub>, Thermal efficiency

## 1. Introduction

Earth's surface is intercepted by the immense source of energy delivered by the sun. It has been seen that earth surface receives around 174 PW of solar energy [1]. Solar collectors are those devices which are useful to tap this source of energy. Various collectors have been discovered from time to time like flat plate collector to concentrating solar collector like parabolic solar collector [2]. Parabolic solar collector are those type of collector in which all the sun rays is made to concentrate over the absorber tube through a reflector [3]. Low thermal conductivity of the conventional working fluid has posed a limitation on the thermal efficiency of such solar collectors. Usage of nanofluids as a working fluid in such collector greatly helps in improving the thermal efficiency, due to their better thermal properties over conventional fluids like water [4]. Nanofluids are basically a suspension of solid nanomaterials of fine size and shape like copper, aluminium, gold, silver etc and their corresponding oxides in base fluid of a conventional fluid [5]. Since solids have a high thermal conductivity, so it can be expected that thermal conductivity of the nanofluids is also better than the conventional fluid, as

they contains the solid nanomaterials in a suspended form. Other benefits of using nanofluid as working fluid are that: a) they have got better absorptance ability in the solar range, while in infrared range their emissivity is low. Moreover intermediate stage of heat transfer which is accompanied by various heat losses are avoided, as the solar energy is absorbed directly by the nanofluid which all together is helpful in enhancing the performance of solar collector using nanofluid as main working fluid [6].

Recently many researchers have conducted both experimental and theoretical analysis of nanofluid based solar collector in order to predict the efficiency of such collector. Yousefi *et al.*[7] have used Al<sub>2</sub>O<sub>3</sub> nanoparticles for the preparation Al<sub>2</sub>O<sub>3</sub>-H<sub>2</sub>O nanofluid. This prepared sample was used as a working fluid in flat plate solar collector, and it was found that efficiency of collector got improved by 28.3% at 0.2 wt% of nanofluid as compared with water. Otanicar *et al.*[8] carried out both experimental and the CFD investigations with different types of nanofluids like carbon nanotubes, graphite and silver, in order to study their effect on the system performance. It was concluded that by using

graphite nanoparticles having an average size of 30 nm, performance of the DASC was increased up to 3% as compared with conventional working fluid. It was also found out that with decrement in the size of silver particle from 40 nm to 20 nm, an improvement of about 6% in the efficiency of solar collector was seen. Han *et al.*[9] carried out comparative analysis on the efficiency of tubular solar collector with three different nanofluids consisting of  $Al_2O_3$ , ZnO and MgO in water based and it was found out that that the nanofluid of ZnO-water at 0.2% volume concentration was a better selection as working fluid in the solar collector than other tested nanofluids. Saini *et al.*[10] carried out an experiment with nanofluid of single wall carbon nanohorns (SWCNH) dispersed in water to investigate their thermal and optical characteristics in view of their use as working fluid in solar collector device. It was reported that their thermal conductivity was higher as compared with conventional water. Photonic properties of the fluid containing SWCNHs were also improved too much extent which was confirmed by spectral transmission measurement. Taylor *et al.*[11] carried out both experimental and theoretical investigation in order to evaluate the performance of nanofluid as working fluid in high flux solar collectors. The result showed that when graphite-therminol VP-1 nanofluid with a volume concentration of 0.01% nanofluid was used as a working fluid in solar collector, an improvement in efficiency of about 10% was seen as compared to water. Marcatelli *et al.*[12] performed experimental investigation in order to study both absorption and the scattering properties of carbon nanohorns nanoparticles dispersed in an aqueous solution of water for the usage as a working fluid in solar collector. The different morphologies of carbon nanohorns like: dahlia, bud, seed were taken during the investigation. Surfactant was also used for the preparation of sample. From the scattering results it was revealed that the only small portion of light (less than 5%) was scattered by the single walled carbon nanohorns-water based nanofluid. It means as high as 95% of the incoming solar radiations will be absorbed by the fluid, which in turns improves the system efficiency. Khullar *et al.*[13] evaluate the environmental impact of nanofluid based concentrating solar water heating system (NCSWHS). Possible application of nanofluid as a working fluid in NCSWHS was also presented. The performance of NCSWHS was found to be better than that of water based solar water heating system, as better output in terms of greater outlet temperature of the working fluid was seen with the usage of nanoparticle in base fluid of solar collector as compared with simple base fluid. From the environmental aspects, greater reduction in the  $CO_2$  level and other green houses responsible for global warming was also seen with the usage of nanofluid as a main working fluid in solar collector system. Moghadam *et al.*[14] conducted experimental analysis on the flat plate solar collector using copper oxide-water ( $CuO-H_2O$ ) nanofluid. Comparison in terms of collector efficiency was drawn between both conventional fluid like water and a nanofluid ( $CuO-H_2O$ ). Copper-oxide nanoparticle ( $CuO$ ) of an average size of 40 nm was used. Nanofluid of 0.4% volume of fraction at three different mass flows (1 kg/min, 2 kg/min and 3 kg/min) was made to flow inside an absorber tube. It was shown that at mass flow rate of 1kg/min, an improvement of about 21.8% in efficiency of solar collector was seen as compared with

conventional fluid water. It was also concluded that there is an existence of an optimum mass flow rate for particular volume of fraction of nanofluid, at which maximum possible efficiency of the flat plate solar collector will be achieved. Finally it was remarked that enhancement in the efficiency of the solar collector was generally witnessed due to improved thermal properties of the nanofluid, as compared with the normal fluid like water etc.

## 2. Experimental Methodology

Schematic of experimental study is carried out on parabolic solar collector which is shown in the figure 1. Main specifications of the parabolic solar collector are shown in table 1. Experiment is carried out with water and  $Al_2O_3-H_2O$  (DI) nanofluid of four different volume concentrations of 0.05%, 0.075%, 0.1% and 0.125%. Working fluid is made to flow at three different volume flow rates of 30 LPH, 50 LPH and 80 LPH. Main components of parabolic solar collector are: a) Absorber tube: Working fluid is made to flow through it, and it takes up the solar energy during its travel. Absorber tube is made up of copper and it is black coated from outside, so as to absorb more solar energy. b) Reflector: It is made up of parabolic shape using mirror strips, where it reflects and concentrates the solar radiations towards the absorber tube. c) Ball valve: It is used to regulate the flow. d) Storage tank: It is used to store the working fluid and it is well insulated using glass wool and insulating sheet, in order to avoid the heat transfer losses and e) Piping arrangement: It is used to circulate the working fluid within the closed system of parabolic shaped concentrating solar collector.

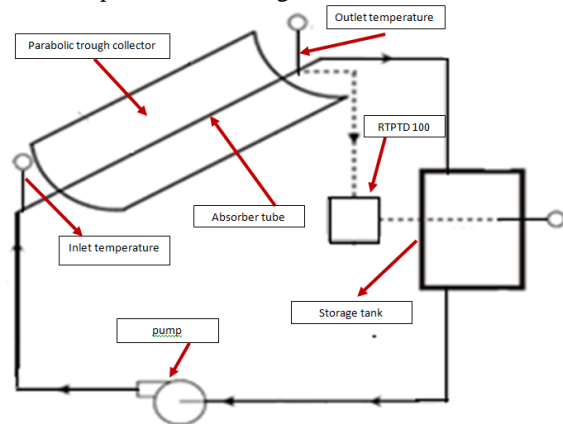


Figure 1. Schematic of experimental study

### 2.1 Working procedure

Working fluid from the storage tank is made to circulate using pump placed within the storage tank. Piping arrangement with the insulating sheets is used to carry the working fluid from the storage tank to the ball valve, where flow is regulated and then desired flow is made to enter into the absorber tube, from where the working fluid picks up the solar energy which is falling directly and concentrated upon absorber tube using reflector. From the absorber tube, working fluid of increased internal energy is then made to enter into the storage tank, and from where process is repeated. Both inlet and outlet temperature are recorded using thermometers which are place at both inlet and outlet sections of the absorber tube. Solar intensity is measure using solar power meter, while wind

velocity is measure using anemometer. All the readings are taken from 9.30 am to 2.30 pm with an interval of 30 minutes.

**Table 1.** Specifications of parabolic shaped concentrating solar collector

Parameter	Value
Collector length, L	1.20 m
Collector breadth, W	0.915 m
End plate thickness	2 mm
Aperture area, $A_{aper}$ .	1.0188 m <sup>2</sup>
Rim angle	90 °
Focal length	0.30 m
Receiver inside diameter ( $D_i$ )	0.027 m
Receiver outside diameter ( $D_o$ )	0.028m
Receiver length	1 m
Glass envelope inside diameter, ( $D_{ci}$ )	0.064 m
Glass envelope outside diameter, ( $D_{co}$ )	0.066 m
Insulation on pipes	Aluminum foil, Superlon
Concentration ratio, $C_r$	9.66

### 2.2 Nanofluid preparation

One step method is used for the preparation of nanofluid, where  $\alpha$ -  $Al_2O_3$  nanoparticles of 20 nm average size of desired amount is made to mix with water in order to form nanofluid of desired volumetric concentration (0.05%, 0.075%, 0.1% and 0.125%) and then this sample is stirred in magnetic stirrer for 30 minutes and afterwards sample is place in ultrasonicator. Where, ultrasonic rays break up the nanoparticles, so that finely suspended nanofluid is prepared. The various specifications of the used nanoparticle are shown in table 2. TEM image of the  $\alpha$ - $Al_2O_3$  nanoparticle is shown in figure 2.

**Table 2.** Physical properties of  $\alpha$ - $Al_2O_3$  nanoparticle

Chemical name	Alumina Nanopowder
Particle size	20-30 nm
Particle shape	Spherical
Appearance	White
pH value	6.6
Density	3.97 gm/cm <sup>3</sup>
Specific surface area	15-20 m <sup>2</sup> /gm
Crystal form	Alpha

High purity	99%
Thermal conductivity of particle	36 W/ m-K
Special heat of particle	765 J/ kg-K

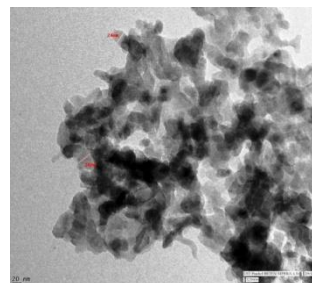


**Figure 2.** TEM image of  $\alpha$ - $Al_2O_3$  nanoparticles

Amount of  $\alpha$ - $Al_2O_3$  nanoparticle required for the preparation of nanofluid of desired volumetric concentration is calculated from the following equation:

$$f_v = V_{np} / V_{nf} \tag{1}$$

Where:  $V_{np} = W_{np} / \rho_{np}$

$$V_{nf} = V_{np} + V_{bf}$$

$$V_{bf} = W_{bf} / \rho_{bf}$$

Expression in a modified form is given as:

$$f_v = \frac{V_{np}}{V_{np} + V_{bf}} = \frac{W_{np} / \rho_{np}}{(W_{np} / \rho_{np}) + W_{bf}} \tag{2}$$

Where,  $V_{np}$  is quantity of nanoparticle,  $V_{bf}$  = quantity of base fluid,  $V_{nf}$  is quantity of nanofluid,  $W_{np}$ =weight of the nanoparticle and  $W_{bf}$  is weight of nanofluid

Table 3 shows the amount of  $\alpha$ - $Al_2O_3$  nanoparticles required for the preparation of nanofluid of desired volumetric concentration. Figure 3 shows various prepared sample of  $Al_2O_3$ - $H_2O$  (DI) nanofluid of various different volumetric concentrations

**Table 3.** Required amount of nanoparticle (grams)

Volumetric concentration %	mass of nanoparticles (grams) for 1 liter
0.05%	1.985
0.075%	2.9775
0.1%	3.970
0.125%	4.9625



**Figure 3.** Various prepared working fluid: (a) Distilled water, (b) 0.05% vol. conc. Al<sub>2</sub>O<sub>3</sub>-H<sub>2</sub>O (DI), (c) 0.075% vol. conc. Al<sub>2</sub>O<sub>3</sub>-H<sub>2</sub>O (DI), (d) 0.1% vol. conc. Al<sub>2</sub>O<sub>3</sub>-H<sub>2</sub>O (DI), (e) 0.125% vol. conc. Al<sub>2</sub>O<sub>3</sub>-H<sub>2</sub>O

Various thermo-physical properties of the nanofluid are evaluated using following mathematical modelling equations:

1. Density of nanofluid [15]  

$$\rho_{nf} = f_v \rho_{np} + (1 - f_v) \rho_{bf} \quad (3)$$

Where  $\rho_{np}$ ,  $\rho_{nf}$ ,  $\rho_{bf}$ , are the density of nanoparticle (kg/m<sup>3</sup>), density of nanofluid (kg/m<sup>3</sup>), density of base fluid (kg/m<sup>3</sup>) respectively and  $f_v$  is the volume concentration of nanofluid.

2. Specific heat of nanofluid [16]  

$$C_{nf} = \frac{f_v \rho_{nf} C_{np} + (1 - f_v) \rho_{bf} C_{bf}}{\rho_{nf}} \quad (4)$$

Where:  $C_{nf}$ ,  $C_{np}$ ,  $C_{bf}$  are the specific heat of the nanofluid, nanoparticle and base fluid respectively in J/kg-K.

3. Thermal conductivity of nanofluid [16]  

$$K_{nf} = \left[ \frac{K_{np} + 2K_{bf} + 2f_v(K_{np} - K_{bf})}{K_{np} + 2K_{bf} - f_v(K_{np} - K_{bf})} \right] K_{bf} \quad (5)$$

Where:  $K_{nf}$ ,  $K_{bf}$ ,  $K_{np}$  are the thermal conductivity of the nanofluid, base fluid and nanoparticle respectively in the W/m-K.

4. Dynamic viscosity of nanofluid [15]  

$$\mu_{nf} = \frac{\mu_{bf}}{(1 - f_v)^{2.5}} \quad (6)$$

Where:  $\mu_{nf}$ ,  $\mu_{bf}$  are the dynamic viscosity of the nanofluid and base fluid respectively.

**3. CFD Methodology**

CFD analysis of the absorber tube of the solar collector, where working fluid is made to flow is carried out using ANSYS FLUENT 14.5. Problem is solved in transient state. Following governing equations are solved to obtain the desired results.

a) Continuity equation

$$\frac{\partial \rho}{\partial t} + \frac{\partial(\rho u_i)}{\partial x_i} = 0 \quad (7)$$

b) Momentum equation

$$\frac{\partial(\rho u_i)}{\partial t} + \frac{\partial(\rho u_i u_j)}{\partial x_j} = \frac{\partial}{\partial x_j} \left[ \rho \delta_{ij} + \mu \left( \frac{\partial u_i}{\partial x_j} + \frac{\partial u_j}{\partial x_i} \right) \right] + \rho g_i \quad (8)$$

c) Energy equation

$$\frac{\partial(\rho C_p T)}{\partial t} + \frac{\partial(\rho u_i C_p T)}{\partial x_i} - \frac{\partial}{\partial x_j} \left[ \lambda \frac{\partial T}{\partial x_j} \right] = S_T \quad (9)$$

d) Turbulence Kinetic energy equation:

$$\frac{\partial(\rho k)}{\partial t} + \frac{\partial(\rho k u_i)}{\partial x_i} = \frac{\partial y}{\partial x_j} \left[ \Gamma_k \frac{\partial k}{\partial x_j} \right] + G_k - Y_k + S_k \quad (10)$$

Where,  $u_i$  is time averaged velocity vector,  $\rho$  is density of fluid,  $c_p$  is specific heat of fluid,  $T$  is temperature,  $\delta_{ij}$  is kronecker delta function,  $G_k$  is generation of turbulence KE due to mean velocity gradients,  $Y_k$  represents contribution of fluctuating dilatation in compressible turbulence to overall dissipation rate.  $\lambda$  is bulk viscosity coefficient,  $x_i$  and  $x_j$  are spatial coordinate,  $k$  is thermal conductivity of the fluid,  $\mu_t$  is eddy viscosity and  $\Gamma_k = (\mu_t / \sigma_k)$  and  $S_k$  is transport of KE due to diffusion.

Following depicted methodology is adopted for carrying out CFD simulation

**3.1 Geometry modelling of absorber tube (HCE)**

First of all the 3-D geometry of absorber tube (HCE), is drawn in geometry modeler of ANSYS FLUENT 14.5, which is depicted in figure 4. The desired model of the absorber tube consist of two concentric tube one for the heat collector element (fluid domain) in which working fluid is made to flow and other for the glass cover to evacuate the heat absorber tube. The absorber tube is split into two parts: a) upper part and b) lower part of the absorber tube facing the reflector. Upper part receives the incoming direct solar radiation, while lower half part is radiated by the concentrated heat flux from the parabolic shaped reflector.

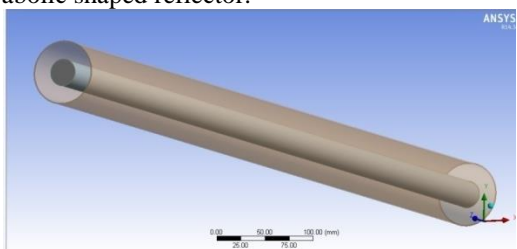


**Figure 4.** Geometry model of HCE (absorber tube)

### 3.2 Mesh generation

Discretization of the geometry is done over created 3-D geometry of the absorber tube which is shown in figure 5. Mesh of hexahedral shape of size 0.3 mm is used over the 3-D geometry. Hexahedral mesh of size 0.3 mm is used because it involves less computational time and optimum accurate results are achieved through it

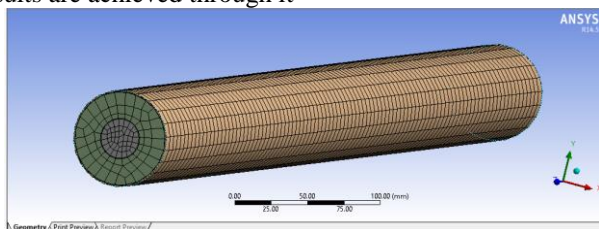


**Figure 5.** Meshed model of HCE (absorber tube)

### 3.3 Material properties

Table 4 shows thermo-physical properties of various materials associated with HCE for carrying out simulation.

### 3.4 Physical Modelling

Various physical models have been applied over a HCE (absorber tube) for carrying out CFD simulation. Physical model applied are depicted below:

- a) Flow behaviour model

K-ε turbulent model is applied, as the Reynolds number for each working fluid is greater than 4000.

- b) Energy model

Energy model is tuned on to visualize the heat transfer effects from the absorber tube. Through the energy model, temperature of the working fluid is specified and heat flux is specified for the wall boundary.

- c) Surface to surface (S2S) radiation model

Surface to surface (S2S) radiation model is used to simulate the radiation heat transfer, which is arising in the closed set of the diffuse surfaces. In the S2S radiation model, the view-factors of the participating zone are calculated. Surface of the outer glass shield and absorber tube are taken into consideration during the calculation of shape factor. S2S radiation model assumes that the surfaces are grey and diffuse i.e. there is no dependency of the wavelength of the incoming radiation on the surface.

- d) Solar load cell

Solar load cell is used for modelling the solar fluxes. In the solar load cell, value of latitude, longitude of the location and date & time of the experiment are specified. Values of the mesh orientation, as desired like negative z axis for the north and while for east positive x-axis is also specified in the solar calculator for the present research. On substitution of all the required inputs in the solar calculator, values for direct normal

solar radiation on the ground, diffuse solar radiation for both vertical and horizontal surface, ground reflected solar radiation for vertical surface and vector for sun direction are obtained. Solar ray tracing is also applied which makes use of both positioning vector of the solar location.

**Table 4.** Thermophysical properties of various materials associated with HCE

Sample material	Density(kg/m <sup>3</sup> )	Specific heat (J/kg-K)	Thermal conductivity (W/m-K)	Viscosity (pa-s)
Water	1000	4187	0.667	4.06e-4
0.05% Al <sub>2</sub> O <sub>3</sub> -H <sub>2</sub> O	1148.5	3595.5	0.766	4.615e-4
0.075% Al <sub>2</sub> O <sub>3</sub> -H <sub>2</sub> O	1227.5	3353.7	0.819	4.933e-4
0.1% Al <sub>2</sub> O <sub>3</sub> -H <sub>2</sub> O	1297	3139.55	0.876	5.283e-4
0.125% Al <sub>2</sub> O <sub>3</sub> -H <sub>2</sub> O	1371.25	2948.59	0.935	5.668e-3
Glass	2200	910	1.75	-
Copper	8.954e3	380	386	-

### 3.5 Boundary conditions

Various boundary conditions applied over absorber tube (HCE) for solving various governing equations is depicted in the table 5.

**Table 5.** Various boundary conditions applied over a HCE

Zone	Boundary condition
Inlet	Mass flow rat inlet and fluid inlet temperature
Outlet	Out flow condition
Upper part of absorber tube	No slip condition and heat flux as modeled by S2S and solar load cell
Lower part of absorber tube facing the absorber tube	No slip condition and heat flux (concentrated by mirror reflector)

### 3.6 Numerical methodology

Different governing equation of mass, momentum and energy are solved through the finite volume method using pressure based segregated spatially implicit solver. Analysis is carried for a transient state in order to simulate the temperature rise within the absorber tube for each set of experimental readings

i.e. from 9.30 am to 2.30 pm with an interval of 30 min. Semi implicit pressure linked equations (SIMPLE) type of pressure correction approach is used for achieving the coupling between momentum and continuity equation, which is used for independent solution of the steady state conservation equations. For solving the momentum and energy equation first order differencing scheme is used. Due to variation in density and presence of swirling type of flows, PRESTO! Scheme is used for interpolation of pressure.

**4. Results and Discussion**

**4.1 Governing Equation for Efficiency Calculation**

Following different governing equations are used for evaluating the parabolic solar collector’s efficiency with different working fluids at different mass flow rates

1) Absorbed Flux  

$$S = G_T R_b (\alpha\tau)\beta Y \tag{11}$$

2) Convective heat transfer coefficient  

$$h_f = Nu \times \frac{k}{D_i} \tag{12}$$

Where:  $Nu = Re^{0.8} Pr^{0.4}$  ;  $Pr = \frac{\mu C_p}{K}$

$$Re = \frac{\rho V D_i}{\mu}$$
 ; 
$$V = \frac{4\dot{m}}{\pi D_i^2 \rho}$$

3) Useful heat gain  

$$q_u = \dot{m} C_p (T_{out} - T_{in}) \tag{13}$$

4) Instantaneous efficiency,  $\eta_i$   

$$\eta_i = \frac{\dot{m} c_p (T_{out} - T_{in})}{G_t R_b W L} \tag{14}$$

5) Thermal efficiency,  $\eta_t$   

$$\eta_t = \frac{\dot{m} c_p (T_{out} - T_{in})}{G_t A_{apper} t} \tag{15}$$

6) Overall efficiency,  $\eta_o$   

$$\eta_o = \frac{\dot{m} c_p (T_{out} - T_{in})}{G_{avg} A_{apper}} \tag{16}$$

Where:  $G_T$  is global solar intensity in  $W/m^2$ ,  $R_b$  is bond resistance,  $\alpha$  is absorptivity of the absorber tube,  $\tau$  is glass cover transmissivity for solar radiation,  $\beta$  is specular reflectivity and  $Y$  is intercept factor,  $Nu$  is Nusselt number,  $K$  is thermal conductivity in  $W/m-K$ ,  $D_i$  is inner diameter of absorber tube in m,  $Pr$  is prandtl number,  $\mu$  is dynamic viscosity in Pa-s,  $C_p$  is specific heat in  $J/kg-K$ ,  $\rho$  is density in  $kg/m^3$ ,  $Re$  is reynolds number,  $V$  is average velocity in m/s and  $\dot{m}$  is mass flow rate in kg/sec,  $W$  is width of the solar collector in m,  $L$  is the length of the absorber tube in m,  $A_{aper}$  is the aperture area of the solar collector in  $m^2$ ,  $t$  is the time duration and  $G_{avg}$  is the average value of solar radiation in  $W/m^2$ .

**4.2 Computational Fluid Dynamics Temperature Contours**

CFD temperature contours with different working fluid (water, 0.05% vol. conc.  $Al_2O_3-H_2O$  (DI) nanofluid, 0.075%

vol. conc.  $Al_2O_3-H_2O$  (DI) nanofluid, 0.1% vol. conc.  $Al_2O_3-H_2O$  (DI) nanofluid and 0.125% vol. conc.  $Al_2O_3-H_2O$  (DI) nanofluid) at a flow rate of 80 LPH is shown in figures 6,7,8,9 and 10 respectively.

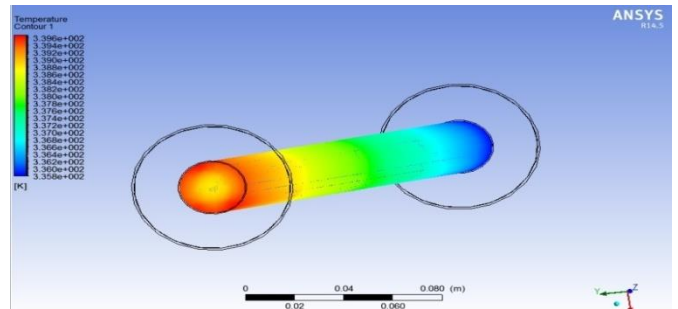


**Figure 6.** Temperature contour with water as a working fluid at 80 LPH

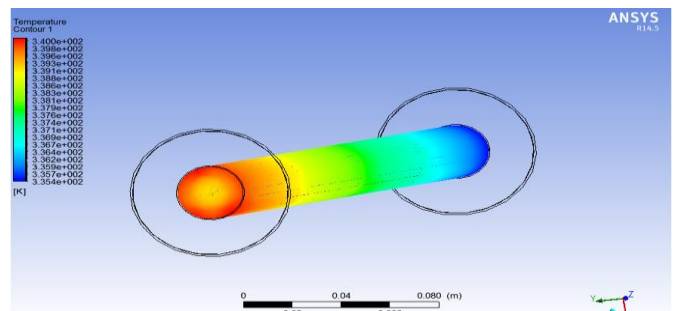


**Figure 7.** Temperature contour with 0.05% vol. conc. alumina-water nanofluid as a working fluid at 80 LPH

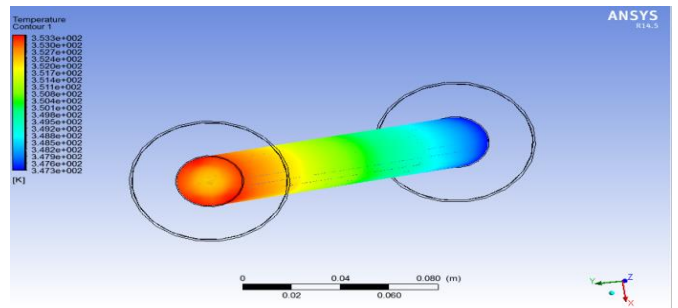


**Figure 8.** Temperature contour with 0.075% vol. conc. alumina-water nanofluid as a working fluid at 80 LPH

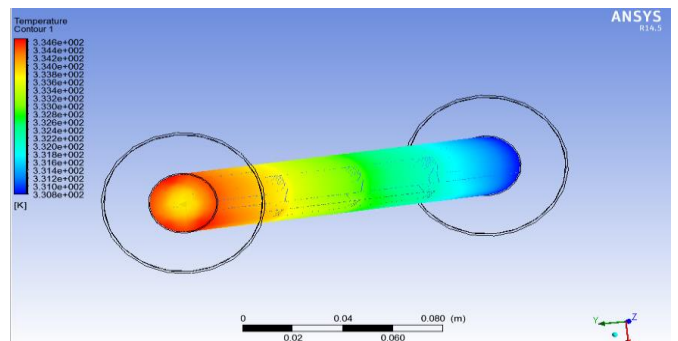


**Figure 9.** Temperature contour with 0.1% vol. conc. alumina-water nanofluid as a working fluid at 80 LPH

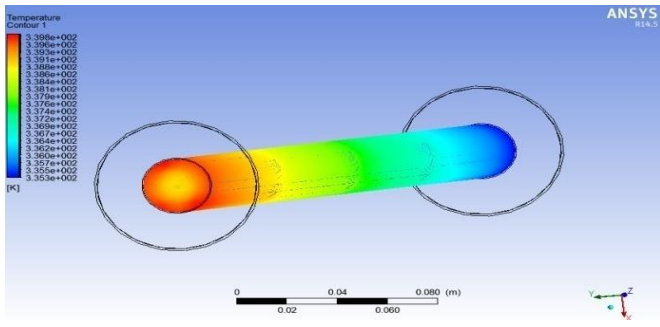


**Figure 10.** Temperature contour with 0.125% vol. conc. alumina-water nanofluid as a working fluid at 80 LPH

4.3 Effect of Mass Flow Rate on Parabolic Solar Collector

Effect of different mass flow rate (30 LPH, 50 LPH and 80 LPH) on the solar collector’s presented in graphs. Where plot of instantaneous efficiency versus reduced temperature parameter  $((T_o+T_i)/2)-T_a)/G_t$  is shown for each working fluid.

4.3.1 Water as a working fluid

Figure 11 shows the variation of both experimental and simulated values of instantaneous efficiency versus reduced temperature parameter  $((T_o+T_i)/2)-T_a)/G_t$  with water as a working fluid at different mass flow rate (30 LPH, 50 LPH and 80 LPH). It is seen that when average of  $T_o$  and  $T_i$  equals  $T_a$  then maximum collector efficiency (experimental) is 17.5%, 31% and 42.5% at 30 LPH, 50 LPH and 80 LPH respectively. While maximum collector efficiency (when average of  $T_o$  and  $T_i$  equals  $T_a$ ) through simulated results is 18%, 32% and 42.5% at 30 LPH, 50 LPH and 80 LPH respectively. It is seen that collector efficiency is enhanced with increasing volume flow rate. Table 6 shows the calculated values of  $F_{RUL}$  and  $F_R(\tau\alpha)$ .

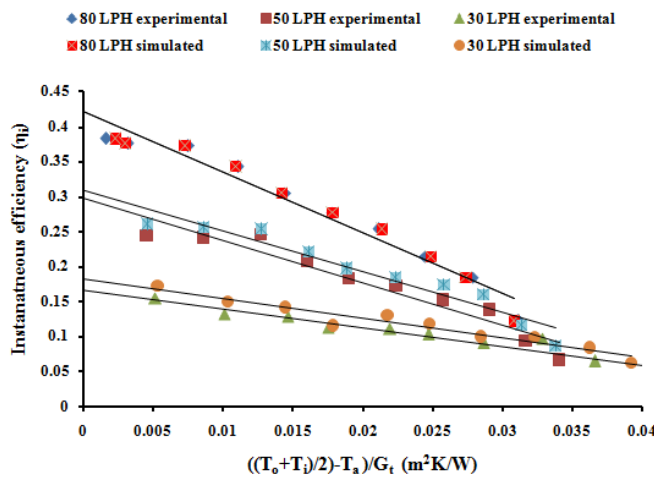


**Figure 11.** Efficiency versus  $((T_o+T_i)/2)-T_a)/G_t$  curve at three flow rate for water

**Table 6.** Collector efficiency parameters at three flow rates for water as working fluid.

Flow rate	Case	$F_{RUL}$	$F_R(\tau\alpha)$
80 LPH	Experimental	8.671	0.421
80 LPH	Simulated	8.671	0.421
50 LPH	Experimental	5.847	0.298
50 LPH	Simulated	6.079	0.309
30 LPH	Experimental	2.694	0.166
30 LPH	Simulated	2.818	0.181

4.3.2 0.05% vol. conc. alumina-water nanofluid as a working fluid

Figure 12 shows the variation of both experimental and simulated values of instantaneous efficiency versus reduced temperature parameter  $((T_o+T_i)/2)-T_a)/G_t$  with 0.05% alumina-water as a working fluid at different mass flow rate (30 LPH, 50 LPH and 80 LPH). It is seen that when average of  $T_o$  and  $T_i$  equals  $T_a$  then maximum collector efficiency (experimental) is 21%, 33% and 52% at 30 LPH, 50 LPH and 80 LPH respectively. While maximum collector efficiency (when average of  $T_o$  and  $T_i$  equals  $T_a$ ) through simulated results is 23%, 34% and 47.5% at 30 LPH, 50 LPH and 80 LPH respectively. It is seen that the collector efficiency is enhanced with increasing volume flow rate. Table 7 shows the calculated values of  $F_{RUL}$  and  $F_R(\tau\alpha)$ .

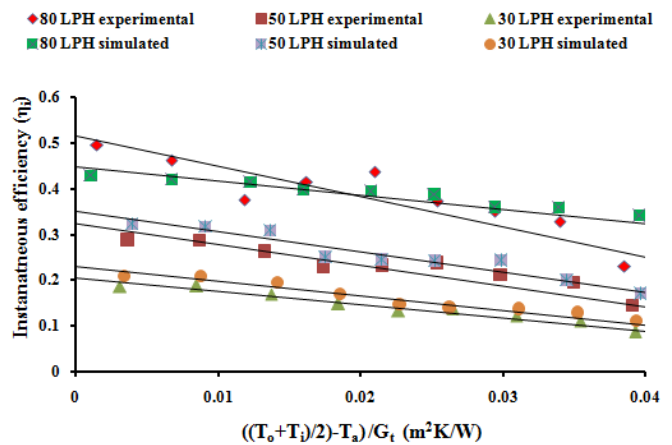


**Figure 12.** Efficiency versus  $((T_o+T_i)/2)-T_a)/G_t$  curve at three flow rate for 0.05% vol. conc. alumina-water nanofluid

**Table 7.** Collector efficiency parameters at three flow rates for 0.05% vol. conc. Al<sub>2</sub>O<sub>3</sub>-H<sub>2</sub>O (DI) as working fluid.

Flow rate	Case	$F_{RUL}$	$F_R(\tau\alpha)$
80 LPH	Experimental	6.607	0.516
80 LPH	Simulated	3.11	0.448
50 LPH	Experimental	4.611	0.325
50 LPH	Simulated	4.460	0.351
30 LPH	Experimental	2.954	0.206
30 LPH	Simulated	3.169	0.229

4.3.3 0.075% vol. conc. alumina-water nanofluid as a working fluid

Figure 13 shows the variation of both experimental and simulated values of instantaneous efficiency versus reduced temperature parameter  $((T_o+T_i)/2)-T_a)/G_t$  with 0.075% alumina-water nanofluid as a working fluid at different mass flow rate (30 LPH, 50 LPH and 80 LPH). It is seen that when average of  $T_o$  and  $T_i$  equals  $T_a$  then maximum collector efficiency (experimental) is 22%, 33% and 64% at 30 LPH, 50LPH and 80 LPH respectively. While maximum collector efficiency (when average of  $T_o$  and  $T_i$  equals  $T_a$ ) through simulated results is 25%, 37% and 72% at 30 LPH, 50 LPH and 80 LPH respectively. It is seen that the collector efficiency is enhanced with increasing volume flow rate. Table 8 shows the calculated values of  $F_{RUL}$  and  $F_R(\tau\alpha)$ .

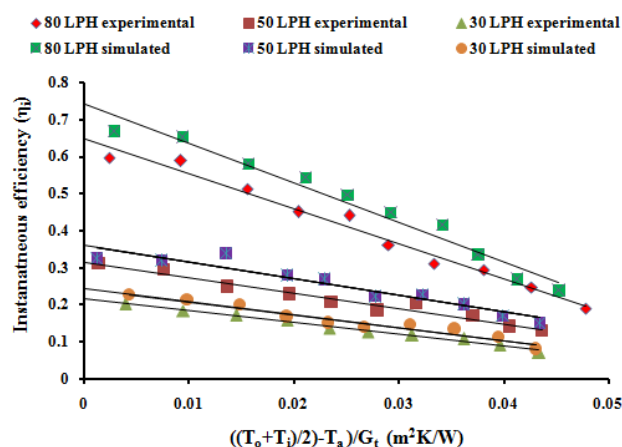


Figure 13. Efficiency versus  $((T_o+T_i)/2)-T_a)/G_t$  curve at three flow rate for 0.075% vol. conc. alumina-water nanofluid.

Table 8. Collector efficiency parameters at three flow rates for 0.075% vol. conc.  $Al_2O_3-H_2O$  (DI) as working fluid.

Flow rate	Case	$F_{RUL}$	$F_R(\tau\alpha)$
80 LPH	Experimental	9.50	0.65
80 LPH	Simulated	10.66	0.743
50 LPH	Experimental	4.18	0.314
50 LPH	Simulated	4.503	0.360
30 LPH	Experimental	3.190	0.215
30 LPH	Simulated	3.473	0.242

4.3.4 0.1% vol. conc. alumina-water nanofluid as a working fluid

Figure 14 shows the variation of both experimental and simulated values of instantaneous efficiency versus reduced temperature parameter  $((T_o+T_i)/2)-T_a)/G_t$  with 0.1% alumina-water nanofluid as a working fluid at different mass flow rate (30 LPH, 50 LPH and 80 LPH). It is seen that when average of  $T_o$  and  $T_i$  equals  $T_a$  then maximum collector efficiency (experimental) is 22%, 40% and 68% at 30 LPH, 50LPH and 80 LPH respectively. While maximum collector efficiency (when average of  $T_o$  and  $T_i$  equals  $T_a$ ) through simulated results is 25%, 42% and 77% at 30 LPH, 50 LPH and 80 LPH respectively. It is seen that the collector efficiency is enhanced

with increasing volume flow rate. Table 9 shows the calculated values of  $F_{RUL}$  and  $F_R(\tau\alpha)$

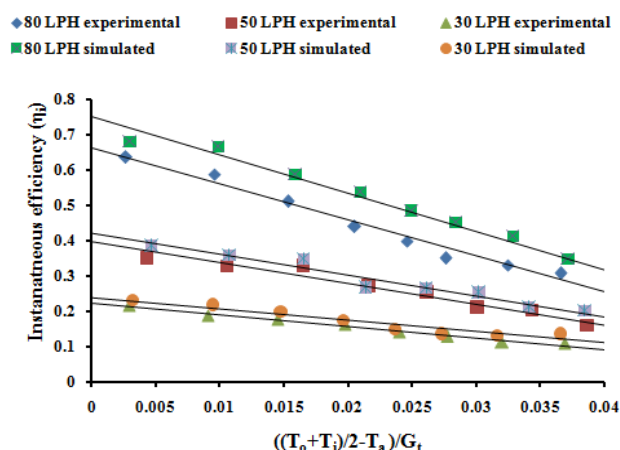


Figure 14. Efficiency versus  $((T_o+T_i)/2)-T_a)/G_t$  curve at three flow rate for 0.1% vol. conc. alumina-water nanofluid

Table 9. Collector efficiency parameters at three flow rates for 0.1% vol. conc.  $Al_2O_3-H_2O$  (DI) as working fluid.

Flow rate	Case	$F_{RUL}$	$F_R(\tau\alpha)$
80 LPH	Experimental	10.26	0.664
80 LPH	Simulated	10.39	0.754
50 LPH	Experimental	5.903	0.397
50 LPH	Simulated	5.898	0.421
30 LPH	Experimental	3.283	0.223
30 LPH	Simulated	3.196	0.239

4.3.5 0.125% vol. conc. alumina-water nanofluid as a working fluid

Figure 15 shows the variation of both experimental and simulated values of instantaneous efficiency versus reduced temperature parameter  $((T_o+T_i)/2)-T_a)/G_t$  with 0.125% alumina-water nanofluid as a working fluid at different mass flow rate (30 LPH, 50 LPH and 80 LPH). It is seen that when average of  $T_o$  and  $T_i$  equals  $T_a$  then maximum collector efficiency (experimental) is 26%, 40% and 71.5% at 30 LPH, 50LPH and 80 LPH respectively. While maximum collector efficiency (when average of  $T_o$  and  $T_i$  equals  $T_a$ ) through simulated results is 28%, 44% and 80% at 30 LPH, 50 LPH and 80 LPH respectively. It is seen that the collector efficiency is enhanced with increasing volume flow rate. Table 10 shows the calculated values of  $F_{RUL}$  and  $F_R(\tau\alpha)$ .

Table 10. Collector efficiency parameters at three flow rates for 0.125% vol. conc.  $Al_2O_3-H_2O$  (DI) as working fluid.

Flow rate	Case	$F_{RUL}$	$F_R(\tau\alpha)$
80 LPH	Experimental	7.954	0.795
80 LPH	Simulated	7.480	0.713
50 LPH	Experimental	5.538	0.398
50 LPH	Simulated	5.874	0.426
30 LPH	Experimental	3.190	0.235
30 LPH	Simulated	3.715	0.271

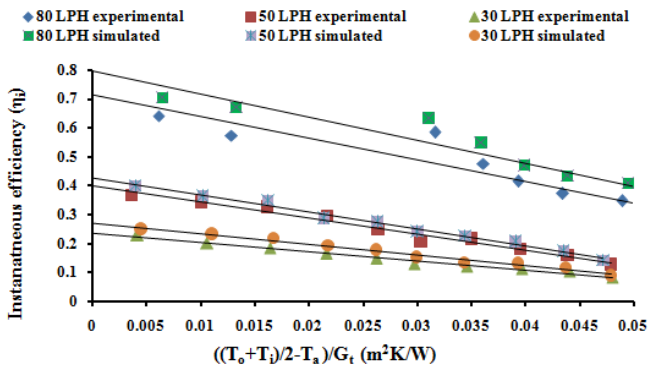


**Figure 15.** Efficiency versus  $((T_o+T_i)/2 - T_a)/G_t$  curve at three flow rate for 0.125% vol. conc. alumina-water nanofluid

4.4 Effect of Different Working Fluids on Solar Collector's Overall Efficiency

Effect of different working fluids on the collector's overall efficiency (both experimental and simulated value) is explain below as

4.4.1 Effect of water and alumina-water based nanofluid of various vol. conc. as a working fluid on collector's overall efficiency at 30 LPH

Figure 16 shows the comparison of water and water based nanofluid of different volumetric concentration at volume flow rate of 30 LPH on collector overall efficiency through both experimental and simulated results respectively. From experimental results it is seen that an improvement of about 7.87%, 8.12%, 9.29% and 9.71% is seen with usage of  $Al_2O_3-H_2O$  nanofluid of 0.05%, 0.075%, 0.1% and 0.125% respectively as compared with water, while from CFD simulated results an improvement of about 8.06%, 8.29%, 8.83% and 10.66% is seen with usage of  $Al_2O_3-H_2O$  nanofluid of 0.05%, 0.075%, 0.1% and 0.125% respectively as compared with water. Moreover there is also a close agreement between both experimental and simulated results.

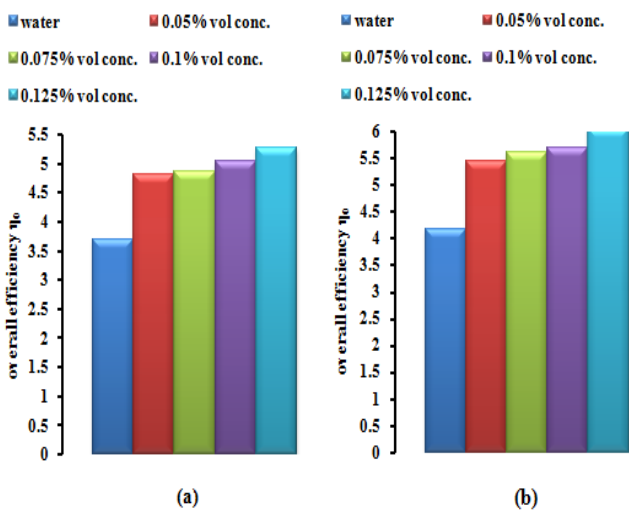


**Figure 16.** Effect of water and alumina-water based nanofluid of various vol. conc. as a working fluid on collector's overall efficiency at 30 LPH (a) Experiential value (b) Simulated value.

4.4.2 Effect of water and alumina-water based nanofluid of various vol. conc. as a working fluid on collector's overall efficiency at 50 LPH

Figure 17 shows the comparison of water and water based nanofluid of different volumetric concentration at volume flow rate of 50 LPH on collector overall efficiency through both experimental and simulated results respectively. From experimental results it is seen that an improvement of about 7.96%, 8.11%, 8.84% and 11.87% is seen with usage of  $Al_2O_3-H_2O$  nanofluid of 0.05%, 0.075%, 0.1% and 0.125% respectively as compared with water, while from CFD simulated results an improvement of about 8.08%, 8.32%, 9.47% and 12.43% is seen with usage of  $Al_2O_3-H_2O$  nanofluid of 0.05%, 0.075%, 0.1% and 0.125% respectively as compared with water. Moreover there is also a close agreement between both experimental and simulated results.

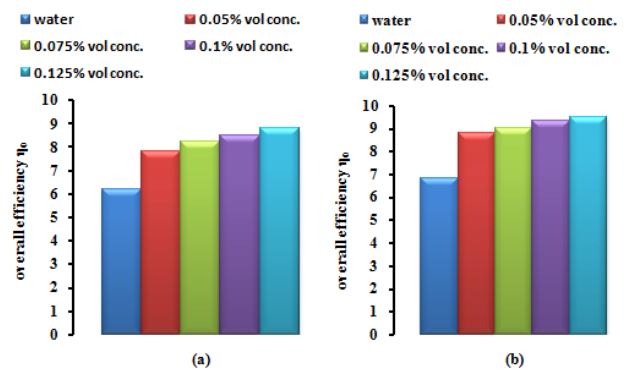


**Figure 17.** Effect of water and alumina-water based nanofluid of various vol. conc. as a working fluid on collector's overall efficiency at 50 LPH (a) Experiential value (b) Simulated value

4.4.3 Effect of water and alumina-water based nanofluid of various vol. conc. as a working fluid on collector's overall efficiency at 80 LPH

Figure 18 shows the comparison of water and water based nanofluid of different volumetric concentration at volume flow rate of 80 LPH on collector overall efficiency through both experimental and simulated results respectively. From experimental results it is seen that an improvement of about 7.98%, 8.31%, 9.40% and 13.98% is seen with usage of  $Al_2O_3-H_2O$  nanofluid of 0.05%, 0.075%, 0.1% and 0.125% respectively as compared with water, while from CFD simulated results an improvement of about 8.23%, 8.87%, 11.19% and 16.84% is seen with usage of  $Al_2O_3-H_2O$  nanofluid of 0.05%, 0.075%, 0.1% and 0.125% respectively as compared with water. Moreover there is also a close agreement between both experimental and simulated results.

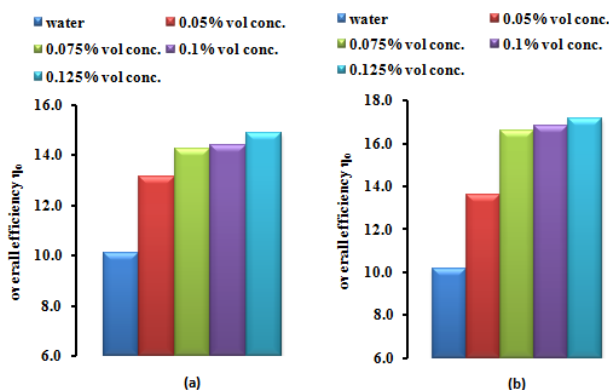


**Figure 18.** Effect of water and alumina -water based nanofluid of various vol. conc. as a working fluid on collector’s overall efficiency at 80 LPH (a) Experiential value (b) Simulated value

### 5. Conclusion

Improvement in both thermal and instantaneous efficiency is reported through both experimental and CFD simulated results, when nanofluid is used as compared to water. Also when volumetric concentration of the nanofluid is made to increase corresponding improvement in the performance of the solar collector is witnessed. With 0.125% vol. conc. Al<sub>2</sub>O<sub>3</sub>-H<sub>2</sub>O (DI) nanofluid at 80 LPH max thermal and instantaneous efficiency of 24.3 % and 68.5% is seen respectively. With the increment in the volume flow rate of the working fluid, corresponding enhancement in the collector’s efficiency also takes place. Improvement of about 18% is seen when the volume flow rate of 0.125% vol. conc. Al<sub>2</sub>O<sub>3</sub>-H<sub>2</sub>O (DI) nanofluid is increased from 30 LPH to 80 LPH. Also, both experimental value of collector efficiency and simulated value of collector efficiency are in close agreement, with a difference of 8%.

### References

[1] Lakalos L., Hevessy G. and Kovacs J., (2011), Advantages and disadvantages of solar energy, “The Journal of General Revolution”, vol. 67, pp. 395-408.  
 [2] Barlev, D., Vidu, R. and Stroeve, P., "Innovation in concentrated solar power", Solar Energy Materials and Solar Cells, Vol. 95 (10), (2011), 2703-2725  
 [3] Reddy K.S., Kumar K.R., (2011), Solar collector field design and viability analysis of standalone parabolic trough power plants for Indian conditions, “Energy for Sustainable Development”, vol. 16 (4), pp. 456-470.  
 [4] Philip John, Shima P.D., (2012), Thermal properties of nanofluids, “Advances in Colloidal and Interface Surface”, vol.10 (4), pp. 30-45.  
 [5] Lee S., Choi S., Li S., Eastman J.A., (1999), Measuring thermal conductivity of fluids containing oxide nanoparticles, “Journal of Heat Transfer”, vol. 121 (2), pp.280-289  
 [6] Wong K.V., De Leon O., (2010), Applications of nanofluids: current and future, “Advances in Mechanical Engineering”, vol. (10), article ID 519659, pp. 1-11 doi: 10.1155/2015/519659

[7] Yousefi T., Veisy F., Shojaeizadeh E., Zinadini S.,(2012c), An experimental investigation on the effect of pH variation of MWCNT-H<sub>2</sub>O nanofluid on the efficiency of a flat plate solar collector, “ Solar Energy”, vol. 86 (2), pp. 771-779.  
 [8] Otanicar T.P., Phelan P.E., Prasher R.S., Rosengarten G., and Taylor R.A., (2010), Nanofluid based direct absorption solar collector, “Journal of Renewable and Sustainable Energy”, vol. 2 (3), pp. 033102-1 to 13.  
 [9] Han D., Meng Z., Wu D., Zhang C., Zhu H., (2011), Thermal properties of carbon black aqueous nanofluids for solar absorption, “Nanoscale Research Letters”, vol. 6, pp. 1-7.  
 [10] Saini E., Mercatelli L., Barison S., Pagura C., Agresti F., Colla L., Sansoni P., (2011), Potential of carbon nanohorns-based suspensions for solar thermal collectors, “Solar Energy Materials & Solar Cells”, vol. 95 (11), pp. 2994-3000.  
 [11] Taylor R.A., Phelan P.E., Otanicar T.P., Adrian R., Prasher R.P., (2011b), Nanofluid optical property characterization towards efficient direct absorption solar collectors, “Nanoscale Research Letters”, vol. 6 (1), pp. 225.  
 [12] Marcatelli L., Saini E., Fontani D., Zaccanti., Martelli F., Di Ninni P., (2011), Scattering and absorption properties of carbon nanohorns-based nanofluids for solar energy applications, “Journal of the European Optical Society- Rapid Publications”, vol. 6, pp. 11025-1 to 5.  
 [13] Khullar V., Tyagi H., (2012a), A study on environmental impact of nanofluid based concentrating solar water heating system, “International Journal of Environmental Studies”, vol. 69 (2), pp. 220-232.  
 [14] Moghadam A.J., Gord M.F., Sajadi M., Zadeh M.H., (2014), Effect of CuO/water nanofluid on the efficiency of a flat plate solar collector, “Experimental Thermal Science”, vol. 58, pp. 9-14.  
 [15] Yousefi T., Veisy F., Shojaeizadeh E., Zinadini S., (2012a), An experimental investigation on the effect of Al<sub>2</sub>O<sub>3</sub>-H<sub>2</sub>O nanofluid on the efficiency of flat plate solar collectors, “ Renewable Energy”, vol. 39, pp. 293-298.  
 [16] Khullar V., Tyagi H., Phelan P.E., Otanicar T.P., Singh H., Taylor R.A., (2012b), Solar energy harvesting using nanofluids-based concentrating solar collector, “Journal of Nanotechnology in Engineering and Medicine”, vol. 3, pp. 031003-1 to 9.